Radial anisotropy in the European mantle: Tomographic studies explored in terms of mantle flow

J. F. Schaefer,[1] L. Boschi,[1,2] T. W. Becker,[3] and E. Kissling[1]

Received 19 September 2011; revised 26 October 2011; accepted 28 October 2011; published 10 December 2011.

[1] Previous studies have shown that radial seismic anisotropy as estimated from flow models is in good agreement with results from tomography at global scale, in particular underlying oceanic basins. However, the fit is typically poor at smaller scale lengths, particularly in tectonically complex regions. We conduct a comparative analysis of tomographically mapped and dynamically modeled radial anisotropy at the scale of Europe and the Mediterranean Basin, including three tomographic models based on different observations and/or methods. We find that adaptive-grid surface-wave tomography, with parametrization density depending locally on the spatial and azimuthal density of data coverage, leads to the seismic model closest to (albeit still far from) geodynamic predictions. The ability to map regional-scale seismic anisotropy may provide a new constraint, complementary to isotropic tomography, to the nature of upper mantle flow.
Citation: Schaefer, J. F., L. Boschi, T. W. Becker, and E. Kissling (2011), Radial anisotropy in the European mantle: Tomographic studies explored in terms of mantle flow, *Geophys. Res. Lett.*, *38*, L23304, doi:10.1029/2011GL049687.

1. Introduction

[2] It is a continuing challenge of geophysical studies to identify a dynamic model of the Earth's mantle that is consistent with surface observables related to plate tectonics [e.g., *Tackley*, 2000]. An important constraint for mantle dynamics is provided by seismic anisotropy, through the relation between strain caused by flow and lattice preferred orientation (LPO) of intrinsically anisotropic grains [e.g., *Montagner*, 2007]. Olivine is the most common upper-mantle mineral with a strong single-crystal anisotropy which makes LPO of anisotropic olivine crystals the main cause of upper-mantle anisotropy [e.g., *Christensen*, 1984; *Silver*, 1996]. Depending on the physical and chemical conditions, i.e., temperature, pressure and water content, different olivine fabrics can be formed according to their preferred slip system. The fabrics vary in their resulting radial anisotropy in strength as well as in pattern. For A- and E-type LPO the fast axes of olivine crystals tend to align in the direction of shear and thus approximately in the direction of mantle flow [*Karato et al.*, 2008]. *Long and Becker* [2010] argue that those may be the dominant fabrics at asthenosphere depth since they allow to achieve a good match between observations of radial anisotropy from seismological studies and geodynamic flow predictions.

[3] A measure of radial anisotropy is the ratio of horizontally (v_{SH}) to vertically (v_{SV}) polarized shear velocity, i.e.,

$$\xi = \left(\frac{v_{SH}}{v_{SV}}\right)^2, \tag{1}$$

so that, in the assumption of A- or E-type LPO, $\xi > 1$ corresponds to horizontal and $\xi < 1$ to vertical flow broadly speaking [e.g., *Karato et al.*, 2008]. Seismic images of lateral changes in anisotropy thus provide us with a unique tool to observe mantle dynamics. A first quantitative exploration of global radial anisotropy in the content of flow models was conducted by *Becker et al.* [2008] who showed good agreement at global scales, with implications for mantle rheology.

[4] Model FMADVOXEU by *Schaefer et al.* [2011] is the first surface-wave-based, radially anisotropic model of the upper mantle to enjoy an adaptive-resolution parametrization, only fine in regions that are sufficiently well covered by the data [*Bijwaard et al.*, 1998].

[5] We interpret maps of radial anisotropy from FMADVOXEU′ in terms of mantle flow. We first evaluate through synthetic tests how well ξ is resolved by FMADVOXEU′ in the European/Mediterranean upper mantle. In a second step, we compare the FMADVOXEU′ map of ξ with the radially anisotropic tomographic models of *Boschi et al.* [2009] and *Chang et al.* [2010], and with a map of ξ that we obtain from a flow model. The goal of our comparative analysis is to establish which radially anisotropic features of Europe and the Mediterranean Basin are likely robustly determined, and what they can tell us about regional-scale mantle flow in this area.

2. Flow and Anisotropy

[6] We constrain radial anisotropy from calculations of mantle circulation performed with the finite element code CitcomS [*Moresi and Solomatov*, 1995; *Tan et al.*, 2006; *Zhong et al.*, 2000]. The modeling approach is the same as that of *Faccenna and Becker* [2010] with modeling assumptions and details described there. We assume the same, simple viscosity profile of *Faccenna and Becker* [2010] and *Boschi et al.* [2010]; *Faccenna and Becker* [2010] found that changes in the pattern of flow caused by deviations from this profile, are small compared to the effect of assumptions about input density models.

[7] As an isotropic velocity model to infer density anomalies we use the Voigt average of model LRSP30EU [*Boschi et al.*, 2009], based on the same database as FMADVOXEU′, but a different (non-adaptive) parametrization. We tested different input models with relatively similar results for estimated

[1]Institute of Geophysics, ETH Zurich, Zurich, Switzerland.
[2]Institute of Theoretical Physics, University of Zurich, Zurich, Switzerland.
[3]Department of Earth Sciences, University of Southern California, Los Angeles, California, USA.

0094-8276/11/2011GL049687

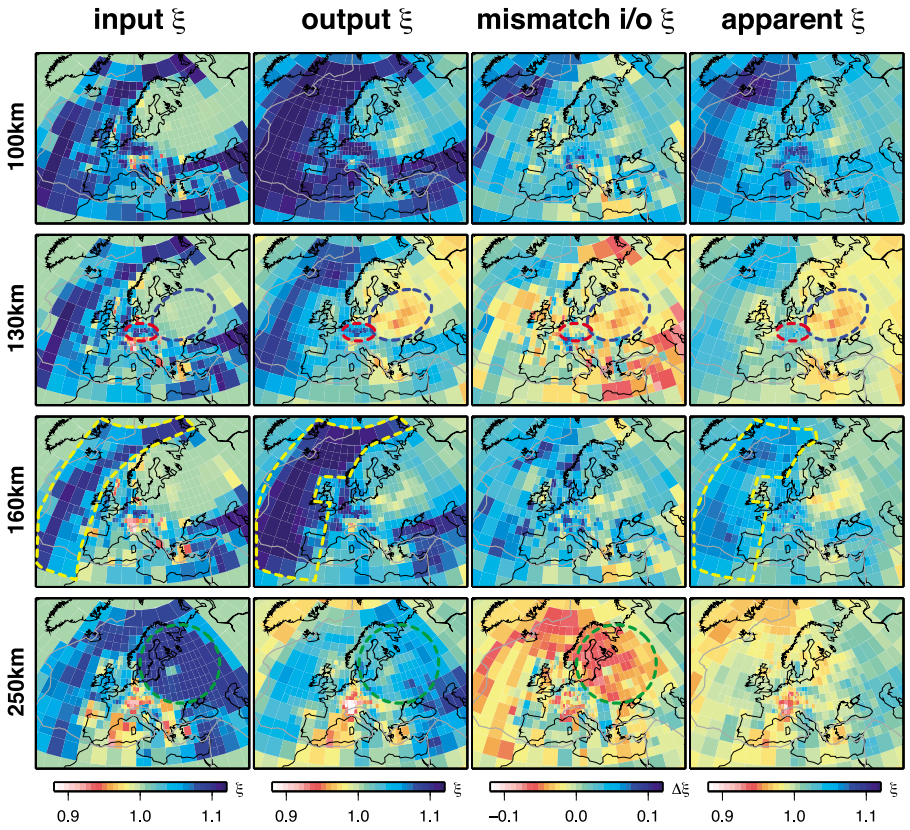

Figure 1. Synthetic test with anisotropic input model. The first column to the left shows the input model of ξ at (top to bottom) 100, 130, 160, 250 km depth. The second column shows the output model at the same depth. The third column is the difference of the input and output model of our first synthetic test, relative to the anisotropic input model. The fourth column is the output of another synthetic test, with a perfectly isotropic input model: we dub this quantity "apparent anisotropy". The red line marks the smallest resolvable feature, the blue one an artifact in the output, the yellow an area where width and amplitude increase as an artifact and the green one a region with decreased amplitude in the output.

radial anisotropy. We decided to present here the results according to LRSP30EU since *Boschi et al.* [2010] show that flow models based on LRSP30EU and other surface-wave-based models achieve a good fit of dynamic topography and micro-plate motions. We thus expect LRSP30EU to deliver an adequate model of regional-scale mantle flow under Europe. It is, however, shown by *Schaefer* [2011] (see in particular Figure 3.3 in section 3 of *Schaefer* [2011]) that a range of different S-velocity models of the region would result in similar flow models.

[8] Following *Becker et al.* [2006, 2008], we compute LPO by tracking velocity gradients along streamlines, via the DREX algorithm of *Kaminski et al.* [2004]. The originally randomly oriented anisotropic grains of an olivine-enstatite assemblage (70/30%) follow tracers until a logarithmic saturation strain of 0.75 is reached for all locations, or until the cut-off age of 60 Ma is reached. Local radial anisotropy is then calculated from Voigt averaging the anisotropy of the LPO-aligned single crystal tensors.

[9] We conduct calculations with and without imposing a high-viscosity keel structure for the thick lithosphere of the Baltic Schild and the East European Platform. The location of this craton is based on 3SMAC [*Nataf and Ricard*, 1996]. The resulting models are nearly isotropic within the craton since strain accumulation is slower due to the higher stiffness (factor 500 compared to ambient mantle), and anisotropy does not form in the allotted time. In reality, the craton might have frozen-in anisotropy from previous tectonic episodes, something we do not account for.

3. Resolution of Tomography

[10] We base our analysis of ξ on a slightly modified version of model FMADVOXEU [*Schaefer et al.*, 2011], merging the two less-well-resolved layers at depths 190 to 300 km into a single, more robustly constrained layer. Like its predecessor our new model FMADVOXEU′ is derived from a database of ~10^6 global teleseismic phase velocity measurements of fundamental-mode Love and Rayleigh waves with a period range between 35 s and 300 s [*Ekström et al.*, 1997; *Boschi and Ekström*, 2002; *Fry et al.*, 2008] which has an especially dense coverage over Europe.

[11] The model is parametrized in a data-adaptive sense [e.g., *Bijwaard et al., 1998*; *Pilidou et al.*, 2004] (latitudinal pixel size varies between 0.625° and 5°) accounting for model resolution capability, estimated by taking the local density of seismic ray paths and their azimuthal coverage into account.

[12] To constrain the reliability of our ξ model we first conduct a resolution test analogous to that of *Schaefer et al.* [2011], but with a realistic input model instead of a simple "checkerboard": namely, the isotropic shear velocity obtained

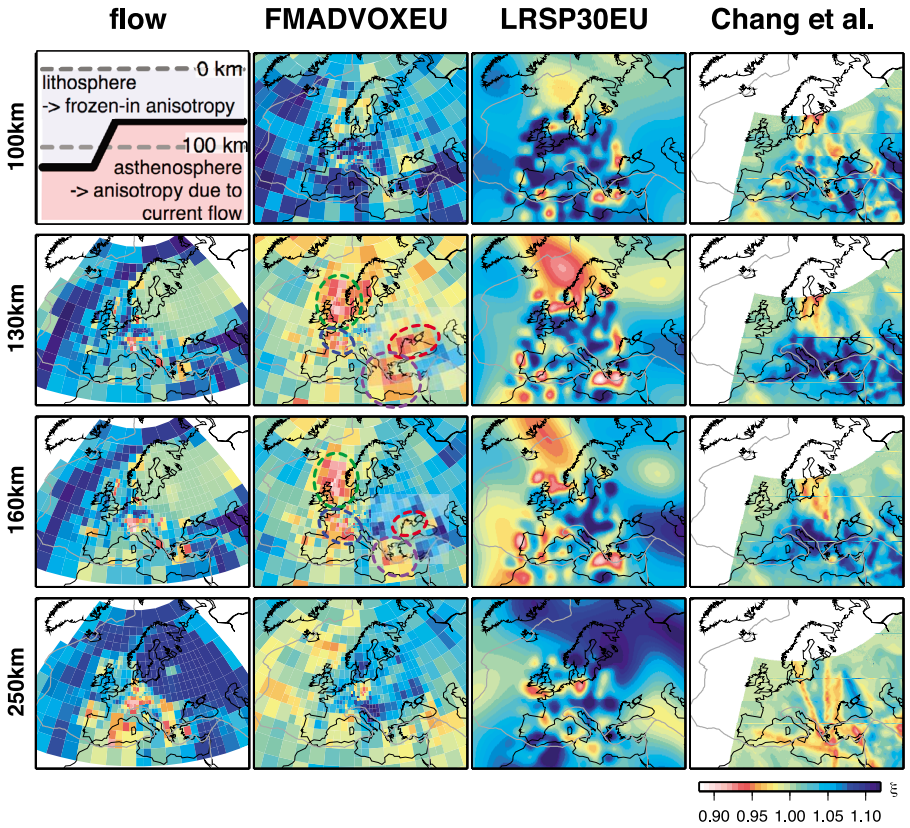

Figure 2. Radial anisotropy for various depths as indicated on the left and derived from four different models from left to right: our flow model, FMADVOXEU′, LRSP30EU of *Boschi et al.* [2009] and the model of *Chang et al.* [2010]. The flow model should not be interpreted directly at a depth of 100 km since this depth falls in the lithosphere where anisotropy is not caused by current flow but is frozen-in after earlier tectonic events. FMADVOXEU′ is characterized by four $\xi < 1$ features marked by dashed circles: (i) North Sea (green), (ii) France (blue), (iii) Hellenic Arc (purple) and (iv) Black Sea (red).

by Voigt-averaging LRSP30EU [*Boschi et al.*, 2009], combined with ξ from the flow model described above. We compute a synthetic database with the same data coverage of *Schaefer et al.* [2011], add Gaussian noise with a standard deviation of 10 s (rough estimate of error based on those of *Ekström et al.* [1997] and *Visser et al.* [2008a, 2008b]), and invert it on the same grid, applying the same amount of damping as with real data.

[13] Because Love waves are primarily sensitive to v_{SH}, and Rayleigh waves to v_{SV} and independently observed differences in their resolution capability can result in apparent anisotropy. To estimate the amount of this induced anisotropy we conduct a second synthetic test like the one described above but with a completely isotropic input model (same as above, but ξ everywhere set to 1, Voigt average of model above is used for v_{SV} and v_{SH}).

[14] In Figure 1 we compare the input map of ξ (first test) with output maps of ξ obtained from the two tests and the mismatch of the output relative to the input. In general the main input features are well resolved, but amplitudes are not well mapped, mainly due to the influence of apparent anisotropy. Apparent anisotropy is largest at or below 250 km depth, which might be related to the sensitivity to v_{SH} decreasing faster with depth than to v_{SV} [e.g., *Schaefer et al.*, 2011].

[15] The $\xi > 1$ feature in Germany is the smallest feature that can be mapped reliably from 100 km to 160 km depth. We can resolve well, in pattern though not in amplitude, the $\xi < 1$ features along the Hellenic arc at 100–250 km depth; north of the Alps at 100–250 km depth; and east of Great Britain at 100–160 km depth. An artificial broadening and increase in amplitude, mainly caused by apparent anisotropy, can be observed for the $\xi > 1$ feature to the west of the area parallel to the mid-oceanic ridge. In the area of the craton the output model shows an artifact with $\xi < 1$ corresponding to apparent anisotropy. At larger depth we can observe in the same area a decrease of amplitude. Resolution might not be high enough to reliably interpret features to the north of the Black Sea.

4. Results and Discussion

[16] We compare in Figure 2 maps of ξ derived from our flow model, from the tomography models FMADVOXEU′ (this study), LRSP30EU [*Boschi et al.*, 2009] and that of *Chang et al.* [2010].

[17] We project all models onto voxels of our adaptive grid and compute the voxel-by-voxel correlation at longitudes between −35° and 60°, and latitudes between 30° and 75°, where both tomography and flow model have best resolution (Figure 3). The overall correlation to the flow model increases from ~0 for the model of *Chang et al.* [2010], to 0.14 for LRSP30EU and 0.21 for FMADVOXEU′. At 130 km depth we achieve the best agreement with a correlation increasing from 0.23 for LRSP30EU to 0.35 for FMADVOXEU′; this

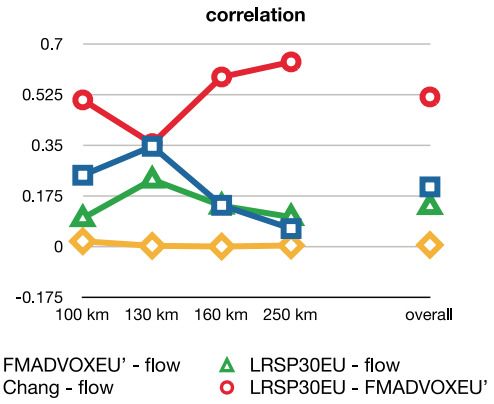

Figure 3. Voxel-by-voxel correlation between the different models (projected onto voxels of our adaptive grid) is calculated for each layer and over all layers in the area of the flow model, for the model of *Chang et al.* [2010] in the available area respectively. The flow model shows best overall correlation as well as in the first three layers with FMADVOXEU′. Correlation of the flow model is in the first two layers significantly higher with FMADVOXEU′ than with LRSP30EU, and values can be compared with the global, long-wavelength correlation which reaches ~0.55 at 200 km depth [*Becker et al.*, 2008].

is also the depth at which the map of ξ from flow models should be most reliable according to *Becker et al.* [2008]. We estimate the significance of correlation (with respect to the null hypothesis of no correlation) implementing equations (14.5.6) and (14.5.10) of *Press* [1992] [see also *Boschi et al.*, 2007]; the number of free parameters to be substituted into those formulae coincides with the number of pixels in our adaptive grid (468 pixels per layer) and therefore accounts for nonuniformity in resolution. Correlation between both FMADVOXEU′ and LRSP30EU with radial anisotropy estimated from flow at 130 km is 99% significant; the overall correlation between FMADVOXEU′ and the estimates from flow is also 99 % significant. Finally, at 130 km depth the mentioned improvement in correlation between LRSP30EU and FMADVOXEU′ is 90 % significant. The actual number of free parameters should in principal be modified to account for regularization, but it would in any case remain $\gtrsim$200, and the significance levels would not change much.

[18] We have conducted the same correlation analysis on all flow models of *Schaefer* [2011], based on different seismic isotropic models. Correlations are relatively high at depth $\lesssim$150 km. All flow models correlate with FMADVOXEU′ better than with other tomography models; none correlates with it better than the one based on LRSP30EU.

[19] LRSP30EU is characterized by strong boundary effects at the border of the high resolution area. The lateral pattern of ξ anomalies in LRSP30EU is dominated by spatial frequencies higher than the isotropic pattern, although, as *Boschi et al.* [2009] note, ξ is generally less well resolved than v_{SH} or v_{SV} alone. Our adaptive-resolution model FMADVOXEU′, which is constrained by the same database, includes longer-wavelength features covering several voxels and more closely comparable to the pattern of regional tectonics and modeled mantle flow. LRSP30EU shows a $\xi < 1$ feature in the North Sea at the boundary of the densely parametrized region which could not have been clearly identified as meaningful, but might have been related to boundary effects. FMADVOXEU′ is now able to reliably map this feature. LRSP30EU and FMADVOXEU′ are based on the exact same data, approximately the same crustal correction (smoothed Crust2.0 vs. exact Crust5.1) and the same software except for the parameterization routines. We infer that, for any typical regional-scale database, radial anisotropy is much better resolved by adaptive-, rather than uniform-grid tomography.

[20] FMADVOXEU′ shows an obvious change in the pattern of ξ below ~100 km, which is probably related to the transition between lithosphere and asthenosphere.

[21] Between 100 and 160 km depth, FMADVOXEU′ is characterized by four $\xi < 1$ features: (i) North Sea, (ii) France, (iii) Hellenic Arc and (iv) Black Sea. A similar pattern of $\xi < 1$ features, with a much smaller lateral extent, emerges from flow modeling; again the narrow north–south $\xi < 1$ shape in the North Sea, the east–west one across eastern France and the Alps, and the two small blobs under the Aegean and north of the Black Sea, at 250 km the North Sea $\xi < 1$ anomaly is not significant anymore.

[22] While we are still far from explaining observed ξ comprehensively in terms of mantle flow, our study suggests that this may become possible with future improvements in seismic data coverage and in tomography and geodynamic modeling. Improving crustal models, to be used as starting points of intermediate-period surface-wave inversions, is essential to high-resolution mapping of anisotropy [e.g., *Ferreira et al.*, 2010], and progress in this sense is expected from current applications of ambient-noise seismology to the European region (e.g., J. Verbeke et al., High resolution tomography of central Europe derived from dense ambient-noise database of Rayleigh waves, submitted to *Geophysical Journal International*, 2011).

5. Conclusions

[23] Our new surface-wave tomography model FMADVOXEU′ is, like FMADVOXEU, based on adaptive parametrization. It is able to map regional-scale radial anisotropy of the tectonically complex European/Mediterranean region (Figure 2). Resolution tests show that the general anisotropy pattern of FMADVOXEU′ is robust in the top 130 km. We can reliably map the Hellenic Arc as well as a feature probably associated to downwelling at the edge of the cratonic lithosphere in the North Sea.

[24] *Becker et al.* [2008] showed that radial anisotropy derived from flow models is in agreement with tomographic studies at very long scale lengths, in regions of simple and smooth tectonics, particularly underneath ocean basins. We have found here that FMADVOXEU′ is correlated at > 90% significance level with expected radial anisotropy based on flow (Figure 2), even in the tectonically complex European/Mediterranean region. The reason for this improvement likely resides in adaptive parameterization, since FMADVOXEU′ and LRSP30EU are based on the same data, theoretical formulation and (approximately) crustal correction.

[25] While we are still far from fully explaining observed ξ in terms of mantle flow, our study suggests that on the basis of seismic models of anisotropy we can expand our toolkit for studies of the dynamics and structure of the lithosphere-asthenosphere system.

[26] **Acknowledgments.** We are thankful to S.-J. Chang, D. Giardini, J.-P. Montagner, M. Panning, M. Wysession and one anonymous reviewers for their careful comments. Most figures are produced using the GMT software of *Wessel and Smith* [1991]. CitcomS was provided by CIG (geodynamics.org) and we thank all contributing authors. Computations were performed on USC's HPCC cluster and partially funded by NSF EAR 0643360.

[27] The Editor thanks Mark Panning and an anonymous reviewer for their assistance in evaluating this paper.

References

Becker, T. W., S. Chevrot, V. Schulte-Pelkum, and D. K. Blackman (2006), Statistical properties of seismic anisotropy predicted by upper mantle geodynamic models, *J. Geophys. Res.*, *111*, B08309, doi:10.1029/2005JB004095.

Becker, T. W., B. Kustowski, and G. Ekström (2008), Radial seismic anisotropy as a constraint for upper mantle rheology, *Earth and Planet. Sci. Lett.*, *267*, 213–227.

Bijwaard, H., W. Spakman, and E. R. Engdahl (1998), Closing the gap between regional and global travel time tomography, *J. Geophys. Res.*, *103*, 30,055–30,078.

Boschi, L., and G. Ekström (2002), New images of the Earth's upper mantle from measurements of surface wave phase velocity anomalies, *J. Geophys. Res.*, *107*(B4), 2059, doi:10.1029/2000JB000059.

Boschi, L., T. W. Becker, and B. Steinberger (2007), Mantle plumes: Dynamic models and seismic images, *Geochem. Geophys. Geosyst.*, *8*, Q10006, doi:10.1029/2007GC001733.

Boschi, L., B. Fry, G. Ekström, and D. Giardini (2009), The European upper mantle as seen by surface waves, *Surv. Geophys.*, *30*(4–5), 463–501.

Boschi, L., C. Faccenna, and T. W. Becker (2010), Mantle structure and dynamic topography in the Mediterranean Basin, *Geophys. Res. Lett.*, *37*, L20303, doi:10.1029/2010GL045001.

Chang, S. J., S. van der Lee, E. Matzel, and H. Bedle (2010), Radial anisotropy along the Tethyan margin, *Geophys. J. Int.*, *182*(2), 1013–1024.

Christensen, N. I. (1984), The magnitude, symmetry and origin of upper mantle anisotropy based on fabric analyses of ultramafic tectonites, *Geophys. J. R. Astron. Soc.*, *76*, 89–111.

Ekström, G., J. Tromp, and E. W. F. Larson (1997), Measurements and global models of surface wave propagation, *J. Geophys. Res.*, *102*, 8137–8157.

Faccenna, C., and T. W. Becker (2010), Shaping mobile belts by small-scale convection, *Nature*, *465*(7298), 602–605.

Ferreira, A. M. G., J. H. Woodhouse, K. Visser, and J. Trampert (2010), On the robustness of global radially anisotropic surface wave tomography, *J. Geophys. Res.*, *115*, B04313, doi:10.1029/2009JB006716.

Fry, B., L. Boschi, G. Ekström, and D. Giardini (2008), Europe-Mediterranean tomography: High correlation between new seismic data and independent geophysical observables, *Geophys. Res. Lett.*, *35*, L04301, doi:10.1029/2007GL031519.

Kaminski, E., N. M. Ribe, and J. T. Browaeys (2004), D-Rex, a program for calculation of seismic anisotropy due to crystal lattice preferred orientation in the convective upper mantle, *Geophys. J. Int.*, *158*(2), 744–752.

Karato, S., H. Jung, I. Katayama, and P. Skemer (2008), Geodynamic significance of seismic anisotropy of the upper mantle: New insights from laboratory studies, *Annu. Rev. Earth Planet. Sci.*, *36*, 59–95.

Long, M. D., and T. W. Becker (2010), Mantle dynamics and seismic anisotropy, *Earth Planet. Sci. Lett.*, *297*, 341–354.

Montagner, J.-P. (2007), Upper mantle structure: Global isotropic and anisotropic elastic tomography, in Treatise on Geophysics, vol. 1, *Seismology and the Structure of the Earth*, edited by G. Schubert and D. Bercovici, pp. 559–589, Elsevier, Amsterdam.

Moresi, L. N., and V. S. Solomatov (1995), Numerical investigation of 2D convection with extremely large viscosity variations, *Phys. Fluids*, *7*, 2154–2162.

Nataf, H. C., and Y. Ricard (1996), 3SMAC: An a priori tomographic model of the upper mantle based on geophysical modeling, *Phys. Earth Planet. Inter.*, *95*, 101–122.

Pilidou, S., K. Priestley, Ó. Gudmundsson, and E. Debayle (2004), Upper mantle S-wave speed heterogeneity and anisotropy beneath the North Atlantic from regional surface wave tomography: The Iceland and Azores plumes, *Geophys. J. Int.*, *159*(3), 1057–1076.

Press, W. (1992), Numerical Recipes in FORTRAN: The Art of Scientific Computing, vol. 1, *FORTRAN Numerical Recipes*, Cambridge Univ. Press, Cambridge, U. K.

Schaefer, J. F. (2011), Adaptively anisotropic tomography of the European upper mantle, Ph.D. thesis, ETH Zurich, Zurich, Switzerland. [Available at http://www.seg2.ethz.ch/scjulia/Julia/publications.html.]

Schaefer, J. F., L. Boschi, and E. Kissling (2011), Adaptively parametrized surface wave tomography: Methodology and a new model of the European upper mantle, *Geophys. J. Int.*, *186*(3), 1431–1453.

Silver, P. G. (1996), Seismic anisotropy beneath the continents: Probing the depths of geology, *Annu. Rev. Earth Planet. Sci.*, *24*, 385–432.

Tackley, P. J. (2000), Mantle convection and plate tectonics: Toward an integrated physical and chemical theory, *Science*, *288*, 2002–2007.

Tan, E., E. Choi, P. Thoutireddy, M. Gurnis, and M. Aivazis (2006), GeoFramework: Coupling multiple models of mantle convection within a computational framework, *Geochem. Geophys. Geosyst.*, *7*, Q06001, doi:10.1029/2005GC001155.

Visser, K., J. Trampert, and B. L. N. Kennett (2008a), Global anisotropic phase velocity maps for higher mode Love and Rayleigh waves, *Geophys. J. Int.*, *172*(3), 1016–1032.

Visser, K., J. Trampert, S. Lebedev, and B. L. N. Kennett (2008b), Probability of radial anisotropy in the deep mantle, *Earth Planet. Sci. Lett.*, *270*, 241–250.

Wessel, P., and W. H. F. Smith (1991), Free software helps map and display data, *Eos Trans. AGU*, *72*(41), 441.

Zhong, S., M. T. Zuber, L. Moresi, and M. Gurnis (2000), Role of temperature-dependent viscosity and surface plates in spherical shell models of mantle convection, *J. Geophys. Res.*, *105*, 11,063–11,082.

T. W. Becker, Department of Earth Sciences, University of Southern California, MC 0740, 3651 Trousdale Pkwy., Los Angeles, CA 90089–0740, USA. (thorstinski@gmail.com)

L. Boschi, E. Kissling, and J. F. Schaefer, Institute of Geophysics, ETH Zurich, Sonneggstrasse 5, CH-8092 Zurich, Switzerland. (boschi@tomo.ig.erdw.ethz.ch; kissling@tomo.ig.erdw.ethz.ch; schaefer@erdw.ethz.ch)